JACS
JOURNAL OF THE AMERICAN CHEMICAL SOCIETY

Article

pubs.acs.org/JACS

Comprehensive Fe–Ligand Vibration Identification in {FeNO}^{6} Hemes

Jianfeng Li,*[,†,‡] Qian Peng,[‡] Allen G. Oliver,[‡] E. Ercan Alp,[§] Michael Y. Hu,[§] Jiyong Zhao,[§] J. Timothy Sage,*[,∥] and W. Robert Scheidt*[,‡]

[†]College of Materials Science and Optoelectronic Technology, University of Chinese Academy of Sciences, YanQi Lake, HuaiRou District, Beijing 101408, China

[‡]Department of Chemistry and Biochemistry, University of Notre Dame, Notre Dame, Indiana 46556, United States

[§]Advanced Photon Source, Argonne National Laboratory, Argonne, Illinois 60439, United States

[∥]Department of Physics and Center for Interdisciplinary Research on Complex Systems, Northeastern University, 120 Forsyth Street, Boston, Massachusetts 02115, United States

Supporting Information

ABSTRACT: Oriented single-crystal nuclear resonance vibrational spectroscopy (NRVS) has been used to obtain all iron vibrations in two {FeNO}^{6} porphyrinate complexes, five-coordinate [Fe(OEP)(NO)]ClO_4 and six-coordinate [Fe(OEP)(2-MeHIm)(NO)]ClO_4. A new crystal structure was required for measurements of [Fe(OEP)(2-MeHIm)(NO)]ClO_4, and the new structure is reported herein. Single crystals of both complexes were oriented to be either parallel or perpendicular to the porphyrin plane and/or axial imidazole ligand plane. Thus, the FeNO bending and stretching modes can now be unambiguously assigned; the pattern of shifts in frequency as a function of coordination number can also be determined. The pattern is quite distinct from those found for CO or {FeNO}^{7} heme species. This is the result of unchanging Fe–N_{NO} bonding interactions in the {FeNO}^{6} species, in distinct contrast to the other diatomic ligand species. DFT calculations were also used to obtain detailed predictions of vibrational modes. Predictions were consistent with the intensity and character found in the experimental spectra. The NRVS data allow the assignment and observation of the challenging to obtain Fe–Im stretch in six-coordinate heme derivatives. NRVS data for this and related six-coordinate hemes with the diatomic ligands CO, NO, and O_2 reveal a strong correlation between the Fe–Im stretch and Fe–N_{Im} bond distance that is detailed for the first time.

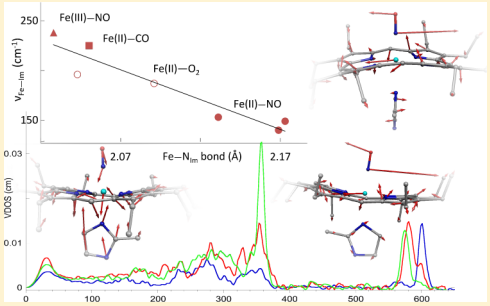

INTRODUCTION

Nitric oxide (NO) is one of three important diatomic ligands (NO, CO, and O_2) that interact with iron porphyrinates.[1] Although the ligands have many common attributes, each ligand can form complexes that have distinct characteristics, and many biological systems are able to distinguish among the three diatomics.[2−5] Uniquely, NO is the only one of the three that will react with iron porphyrinates in both the iron(II) and the iron(III) states. The strong interest in NO as a ligand has led to many investigations and reviews.[6] In addition, the important properties of NO in biology as a messenger and as an immune defense agent are especially significant in the {FeNO}^{7} heme systems.[7,9−20] The five- and six-coordinate {FeNO}^{7} complexes have been studied in some detail;[21] their electronic structures are reasonably well understood and will not be considered further here.

The iron(III) systems ({FeNO}^{6}) have been less intensely studied but also have substantial biological interest especially as insect carriers of NO[22] and in denitrification processes.[23,24] Both five- and six-coordinate species are known. Experimentally, the relatively easy loss of NO from both solutions and solid samples of {FeNO}^{6} complexes, even though the Fe–N(NO) bond is very short (1.64–1.65 Å),[25,26] and easy reductive nitrosylation to {FeNO}^{7} species has made syntheses and characterization challenging.[27] The NO stretching frequency for five-coordinate [Fe(OEP)(NO)]$^{+}$[28] derivatives ranges from 1830 to 1868 cm^{-1}.[29−31] Early characterization revealed unusual spectroscopic properties for six-coordinate species of the type [Fe(Porph)(L)(NO)]$^{+}$, where L is a neutral nitrogen donor such as imidazole or other nitrogen heterocycle. These species had NO stretching frequencies in range of 1890–1921 cm^{-1}, thus bracketing the value of free NO (1876 cm^{-1}).[27] The Mössbauer spectra of the five-coordinate species showed relatively low isomer shifts of ∼0.20 mm/s,[25] whereas the six-coordinate species had unusually low values, ∼0 mm/s,[25] a value in hemes that is usually associated with the oxidation state of +4 for iron.[32] Thus, a description of electronic structures of these seems challenging, an issue to which we will subsequently return. We do note that there are some substantial similarities between the reactions of O_2 and NO with hemes, in particular an unusual spin coupling of paramagnetic reactants. In dioxygen systems, diamagnetic dioxygen complexes are formed from high-spin five-coordinate

Received: October 14, 2014
Published: December 9, 2014

ACS Publications © 2014 American Chemical Society

dx.doi.org/10.1021/ja5105766 | J. Am. Chem. Soc. 2014, 136, 18100–18110

iron(II) hemes and paramagnetic dioxygen;[33] their description has been contentious to this day.[34] In the case of the $[Fe(Porph)(R-Im)(NO)]^+$ species, reaction of a high-spin five-coordinate $[Fe(Porph)(R-Im)]^+$ and paramagnetic NO also forms diamagnetic complexes.

The reported vibrational spectra of six-coordinate $[Fe(Porph)(R-Im)(NO)]^+$ either as proteins or as small molecules have assigned both the Fe−N(NO) stretch and the Fe−N−O bend.[35−38] In all but one case, the stretch is assigned at a higher frequency than the bend. The Fe−N−O bend should be readily distinguished from the stretching mode by two (near) degenerate transitions for the bend; the degeneracy is lifted by the presence of the planar trans ligand. However, the resolution of the bending modes has not been achieved experimentally. Definitive assignments should be obtained by the application of oriented crystal NRVS spectra, which we have recently pioneered[39−42] and which provides detailed orientational, vibrational information. The reported crystallographic properties of five-coordinate $\{FeNO\}^6$ species are appropriate for single-crystal NRVS measurements, but those reported for six-coordinate species are not suitable.

Fortunately, we have isolated a new crystalline form of $[Fe(OEP)(2\text{-}MeHIm)(NO)]^+$ with appropriate crystal symmetry characteristics to allow single-crystal NRVS measurements. This new structure will be described. With appropriate five- and six-coordinate species now available, we have undertaken their oriented single-crystal NRVS that allows the definitive assignment of both the stretching and the bend modes of the axial FeNO group including the resolution of the near degenerate bending modes in $[Fe(OEP)(2\text{-}MeHIm)(NO)]^+$. Vibrational frequencies can be used to illuminate coordination-site and ligand bonding subtleties beyond that discernible by X-ray crystallography alone.[43]

We comment on the stretching and bending patterns of the five- and six-coordinate $\{FeNO\}^6$ species as compared to the five- and six-coordinate $\{FeCO\}^6$ and $\{FeNO\}^7$ species. We have also been able to study and assign the Fe−Im stretching mode across the series of NO, CO, and O_2 iron complexes.

EXPERIMENTAL SECTION

General Information. All reactions and manipulations for the preparation of the iron(III) porphyrin derivatives were carried out under argon using a double manifold vacuum line, Schlenkware, and cannula techniques. Dichloromethane, toluene, and hexanes were distilled under argon over CaH_2 and sodium/benzophenone, respectively. Chlorobenzene was purified by washing with concentrated sulfuric acid, then with water until the aqueous layer was neutral, dried with sodium sulfate, and distilled twice over P_2O_5. 95% $^{57}Fe_2O_3$ was purchased from Cambridge Isotopes. H_2OEP was synthesized by literature methods.[44] Nitric oxide (Mittler Specialty Gases) was purified by fractional distillation through a trap containing 4A molecular sieves bathed in a dry ice/ethanol slurry.[45]

Small-Scale Metalation. Insertion of ^{57}Fe into free-base porphyrins was conducted in purified chlorobenzene according to a modified Landergren method as follows.[46] Approximately 2 mL of 12 M HCl was used to dissolve ∼0.20 mmol 95% ^{57}Fe enriched Fe_2O_3 contained in a 250 mL Schlenk flask. After 5 min of stirring, HCl was removed under vacuum to near dryness, and subsequent steps of the metalation reaction were done in an inert environment using standard Schlenk procedures. Failure to maintain an inert environment will likely result in an incomplete or inefficient metal insertion. One hundred milliliters of freshly distilled chlorobenzene was added via cannula, and the mixture was refluxed for 2 h in a hot oil bath. One-half of the chlorobenzene was removed by distillation, and 10 mL of a chlorobenzene solution containing ∼0.15 mmol of H_2OEP and 0.4 mL of 2,4,6-collidine was added via cannula. After refluxing for 3 h, chlorobenzene was removed under vacuum, and the residue was dissolved in 50 mL of CH_2Cl_2. The solution was washed twice with 50 mL of DI water, thrice with 50 mL of 1 M HCl, and once with 50 mL of DI water. After drying over Na_2SO_4 and filtration through a sintered-glass filter, solvent was removed by rotoevaporation. Minimal CH_2Cl_2 was used to redissolve the product and transfer to an evaporation dish. The remaining solvent was evaporated using very low heat.

Syntheses of $[^{57}Fe(OEP)(NO)]ClO_4$. Single crystals of this complex were prepared as described earlier.[25,26] After metalation as described above, the resulting $[^{57}Fe(OEP)(Cl)]$ was reacted with $AgClO_4$ to produce $[^{57}Fe(OEP)OClO_3]$.[47] To 10 mg (0.014 mmol) of $[^{57}Fe(OEP)OClO_3]$ was added ∼2 mL CH_2Cl_2. NO gas was bubbled into the solution for several minutes. A dramatic color change from brownish-red to purple/pink occurred. A 1:1 mixture of hexanes and CH_2Cl_2 was used as the nonsolvent in the vapor diffusion experiment under an NO atmosphere to obtain X-ray-quality crystals that were used in the single-crystal NRVS experiments.

Caution! Transition metal perchlorates should be handled with great caution and be prepared in small quantities as metal perchlorates are hazardous and may explode upon heating.

Syntheses of $[^{57}Fe(OEP)(2\text{-}MeHIm)(NO)]ClO_4$. Procedures similar to the reported method[48] were used for the single-crystal preparation. Five-coordinate $[^{57}Fe(OEP)(2\text{-}MeHIm)]ClO_4$ was prepared by the reaction of $[^{57}Fe(OEP)OClO_3]$ with 2-MeHIm in methylene chloride.[49] Methylene chloride (0.5 mL) was added to solid $[^{57}Fe(OEP)(2\text{-}MeHIm)]ClO_4$ (12 mg) in an 8 × 150 mm glass tube inside an extra long Schlenk tube under argon. NO gas was bubbled into the solution for 5−6 min. The color of the solution changed from red/brown to purple/pink. X-ray-quality crystals were obtained by layering NO-saturated hexanes over the solution in the tubes. An NO atmosphere must be maintained inside the Schlenk tube during crystallization. These crystal were used in both the X-ray structure determination and the single-crystal NRVS experiments.

X-ray Structure Determination. A black crystal with the dimensions 0.52 × 0.43 × 0.17 mm^3, glued to the tip of a glass fiber, was used for the structure determination at 100 K. Intensity data were collected on a Bruker Apex system with graphite-monochromated Mo Kα radiation (λ = 0.71073 Å). Absorption corrections were based on the multiscan technique as implemented in SADABS.[50] The asymmetric unit contains the full porphyrin cation, the perchlorate anion, and one-half of a dichloromethane molecule. The structures were solved by direct methods using SHELXS-97 and refined against F^2 using SHELXL-97;[51,52] subsequent difference Fourier syntheses led to the location of most of the remaining nonhydrogen atoms. The perchlorate anion was found to be disordered over two distinct orientations at the same crystallographic site with occupancies of 0.684 and 0.316. The solvent molecule is disordered around an inversion center of the unit cell. For the structure refinement, all data were used including negative intensities. All nonhydrogen atoms were refined anisotropically. Hydrogen atoms were idealized with the standard SHELXL-97 idealization methods. Solid-state analysis of crystal packing distances made use of the program MERCURY[53] from the Cambridge Crystallographic Data Center. Complete crystallographic details, atomic coordinates, anisotropic thermal parameters, and fixed hydrogen atom coordinates are given in the Supporting Information for the structure.

NRVS Crystal Mounting. Crystals were mounted onto specially prepared dual arc goniometer heads. Copper wire, 4−5 cm in length and 18 gauge, was affixed to the goniometer and bent into a u-shape. A glass fiber, 5−8 mm in length, was then superglued to project along the goniometer ϕ-axis. The connection of the wire into the goniometer head was fortified with epoxy resin. A crystal was then affixed to the tip of the glass fiber using super glue. The wire was then carefully bent so that the crystal was approximately on the ϕ-axis, and then stretched to the required height for centering. Crystals were then oriented for NRVS analysis along specified in-plane axes by methods described in the Supporting Information.

dx.doi.org/10.1021/ja5105766 | J. Am. Chem. Soc. 2014, 136, 18100−18110

NRVS Spectra. Spectra were measured at Sector 3-ID of the Advanced Photon Source, Argonne National Laboratory, Argonne, IL. Single-crystal samples were previously mounted and aligned on goniometer heads that were screwed into place on a rotating stage. The mounted crystals were then located into the X-ray beam by translations of the stage and rotated to the predetermined ϕ-angle required for the particular direction of analysis desired. A stream of cold N_2 gas from a commercial cryocooler controlled crystal temperature during NRVS measurements. Typical temperatures at the crystal were 100−120 K. Vibrational spectra were measured using an in-line high-resolution monochromator operating at 14.4125 keV with 1.0 meV bandwidth scanning the energy of incident X-ray beam.[54] Spectra were recorded between −30 and 80 meV in steps of 0.25 meV, and all scans (3−6 replicates) were normalized to the intensity of the incident beam and added. NRVS raw data were converted to the vibrational density of states (VDOS) using the program PHOENIX.[39,55] NRVS measurements were made in two orthogonal directions for [^{57}Fe(OEP)(NO)]ClO_4 and three orthogonal directions for [^{57}Fe(OEP)(2-MeHIm)(NO)]ClO_4.

Vibrational Predictions and Predicted Mode Composition Factors e^2. The Gaussian 09 program package[56] was used to optimize the structures and for frequency analysis, with the (BP86)[57] and (M06-L)[58] functionals. In general, we used triple-ζ valence basis sets with polarization functions (TZVP)[59] on iron and 6-31G* for all other atoms. The S = 0 complexes [Fe(OEP)(NO)]$^+$ and [Fe(OEP)(2-MeHIm)(NO)]$^+$ were fully optimized without any constraints using the spin unrestricted DFT method. The starting structure for each was obtained from the crystal structure. Frequency calculations were performed on the fully optimized structures at the same level to obtain the vibrational frequencies of the ^{57}Fe isotopomer. The frequencies reported here were not scaled. The frequency data have been created using the high precision format vibrational frequency eigenvectors to calculate mode composition factors (e^2) and vibrational density of states (VDOS) as described below.

The G09 output files from the DFT calculations can be used to generate predicted mode composition factors with our scripts.[60] The mode composition factors $e^2_{j\alpha}$ for atom j and frequency mode α are the fraction of total kinetic energy contributed by atom j (here, ^{57}Fe, the NRVS active nucleus). The normal mode calculations are obtained from the atomic displacement matrix together with the equation:

$$e^2_{j\alpha,\text{inplane}} = \frac{m_j(r^2_{jx} + r^2_{jy})}{\sum m_i r_i^2} \quad (1)$$

where the sum over i runs over all atoms of the molecule, m_i is the atomic mass of atom i, and r_i is the absolute length of the Cartesian displacement vector for atom i. The polarized mode composition factors are defined in terms of two distinct in-plane directions, which can be calculated from a projection of the atomic displacement vectors x and y (eq 1).[61] The out-of-plane atomic displacement perpendicular to the resulting porphyrin plane for a normal mode is obtained from a projection of the atomic displacement vector z (eq 2).

$$e^2_{j\alpha,\text{outofplane}} = \frac{m_j r^2_{jz}}{\sum m_i r_i^2} \quad (2)$$

The x, y, and z components of the iron normal mode energy for [Fe(OEP)(NO)]$^+$ and [Fe(OEP)(2-MeHIm)(NO)]$^+$ with $\epsilon^2_{Fe} \geq 0.01$ are given in Tables S7, S8 of the Supporting Information.

The predicted mode composition factors $e^2_{j\alpha}$ can also be compared to the integrated spectral areas obtained from NRVS. Therefore, vibrational densities of states (VDOS) can be simulated from the mode composition factors using the Gaussian normal distributions function, where the full width at half height (fwhh) is defined appropriately by considering the spectral resolution in the experiment. In this study, the MATLAB R2010a software was used to generate the predicted NRVS curves.

RESULTS

The X-ray structure of the [Fe(OEP)(2-MeHIm)(NO)]$^+$ cation has been determined; a thermal ellipsoid plot is shown in Figure 1. Also shown in the figure is one of the two orientations of the perchlorate anion. Complete final crystallographic information is given in Tables S1−S6 of the Supporting Information.

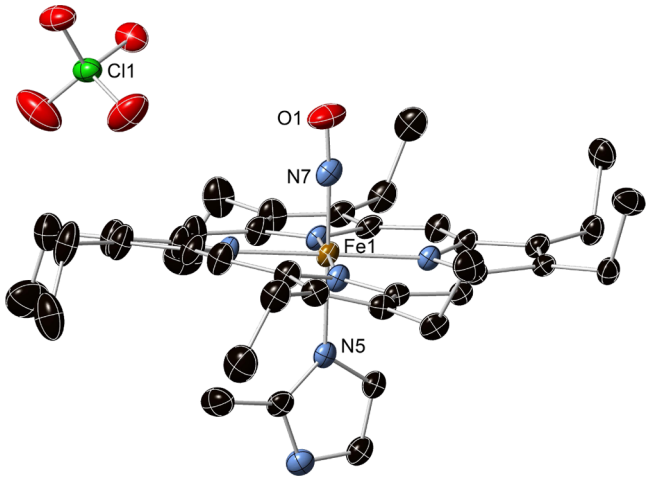

Figure 1. Thermal ellipsoid diagram of the [Fe(OEP)(2-MeHIm)(NO)]$^+$ cation along with the perchlorate counteranion. Ellipsoids are drawn at the 50% probability level. Hydrogen atoms are not shown for reasons of clarity.

Figure 2 displays a formal diagram of the displacement of each atom, in units of 0.01 Å, from the mean plane of the 24-atom core for the [Fe(OEP)(2-MeHIm)(NO)]$^+$ cation. The

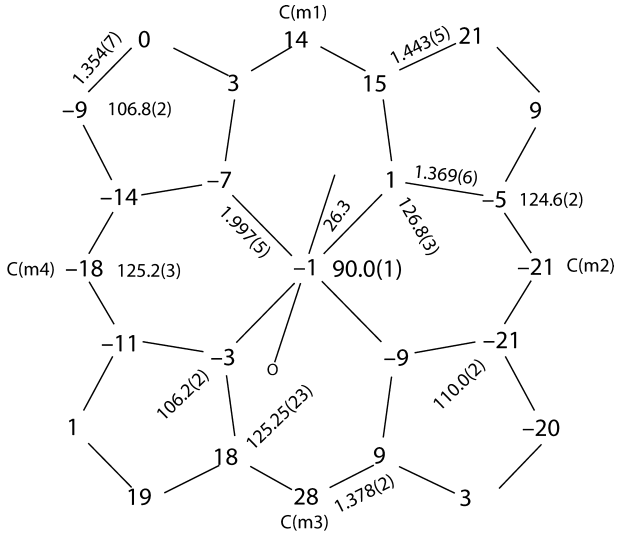

Figure 2. Formal diagram illustrating the deviation of individual atoms (in units of 0.01 Å) from the 24-atom mean plane of the porphyrin core. Positive values of the displacement are toward the NO ligand. The orientation of the *trans* 2-methylimidazole ligand with respect to the porphyrin molecular frame is illustrated by the solid line. The "o" gives the position of the 2-methyl substituent of the imidazole. Averaged values of the chemically unique bond distances (in Å) and angles (in degrees) are shown. The numbers in parentheses are the esd's calculated on the assumption that the averaged values were all drawn from the same population.

dx.doi.org/10.1021/ja5105766 | J. Am. Chem. Soc. 2014, 136, 18100−18110

core conformation is moderately ruffled with the iron atom effectively centered in the porphyrin plane. Figure 2 also gives average bond distances and bond angles for the core atoms. Standard uncertainties, calculated on the assumption that all values are drawn from the same population, are given in parentheses following each averaged value.

Oriented single-crystal NRVS spectra were obtained for the five-coordinate [Fe(OEP)(NO)]$^+$ and six-coordinate [Fe(OEP)(2-MeHIm)(NO)]$^+$ derivatives. Three distinct crystal orientations were measured for [Fe(OEP)(2-MeHIm)(NO)]$^+$: either perpendicular to the porphyrin plane or parallel to the porphyrin plane and either perpendicular or parallel to the axial imidazole plane. Figure 3 shows these experimental oriented

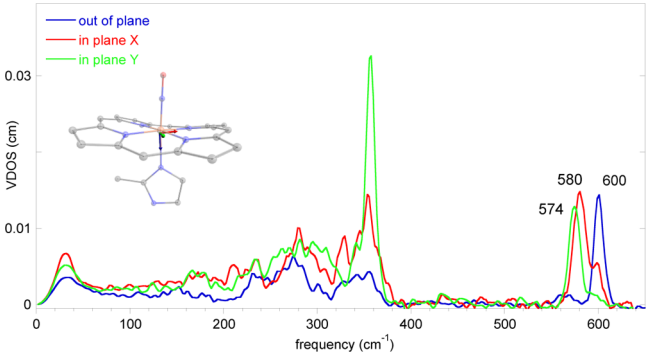

Figure 3. NRVS data obtained on the three orthogonal directions for [Fe(OEP)(2-MeHIm)(NO)]$^+$.

crystal vibrational spectra. In the high frequency region from ~570−610 cm^{-1}, one strong vibration is seen in each of the three measured directions. Because the stretch and bend modes are expected to be the highest frequencies for iron vibrations, the oriented crystal spectra show the Fe−NO stretch as the out-of-plane mode, and the other two in-plane modes, parallel and perpendicular to the imidazole plane, must be the two near-degenerate Fe−N−O bending modes. These vibrational measurements show that in powder (isotropic) measurements the three peaks will typically either be poorly resolved or not resolved at all. Thus, the unresolved powder peaks for the stretching and bending modes seen by Praneeth et al.[37] and Moeser et al.[38] are not unexpected.

Two distinct orientations for five-coordinate [Fe(OEP)(NO)]$^+$ were measured, one with the analyzing beam along the perpendicular to the heme plane and a second with the beam in the porphyrin plane (which is orthogonal to the first). The results are shown in the Discussion and provide all data required for the assignment of the FeNO stretching and bending modes.

Both sets of measurements provide direct evidence for making in-plane versus out-of-plane assignments; in particular, such measurements are seen to be the most appropriate way to provide for the unambiguous assignment of the FeNO stretching and bending modes.

DISCUSSION

X-ray Structure. All previously known crystalline forms of [Fe(Porph)(R−Im)(NO)]$^+$ derivatives are not appropriate for a complete, detailed oriented single-crystal NRVS study. Such a study requires a crystalline form in which the porphyrin planes are all parallel and all molecules have the same orientation (molecules related by inversion symmetry acceptable). Fortunately, we have been able to obtain a new crystalline form of [Fe(OEP)(2-MeHIm)(NO)]ClO_4 that meets these criteria and does allow measurements in three distinct directions defined in the coordinate frame of the molecule. This is illustrated in Supporting Information Figure S1. We briefly note the structural features of this new crystalline form. Table 1 provides structural data for related {FeNO}^{6} and Fe^{II}CO complexes, where the trans ligand (when present) is an imidazole species. Comparison of [Fe(OEP)(2-MeHIm)(NO)]ClO_4 with these data shows the expected close agreement: an effectively linear FeNO group with a short Fe−N(NO) bond (1.641(2) Å), and a trans Fe−N_{Im} bond distance of 2.028(2) Å. An interesting feature is the Fe−N_{Im} bond distances to the sterically hindered 2-MeHIm. As seen in Table 1, the Fe−N_{Im} hindered bond distances range from 2.028 to 2.053 Å, lengths comparable to the Fe−N_{Im} distances to unhindered imidazoles in CO complexes and much shorter than those to hindered imidazole CO species. Thus, both axial

Table 1. Selected Structural Parameters of {FeNO}^{6} Porphyrin Complexes and Related [Fe(Porph)(L)(CO)] Complexes[a]

complex	Δ_{24}[b,c]	(Fe−N_p)$_{av}$[d]	Fe−X_{XO}[c,e]	X−O[c]	Fe−N_{Im}[c]	∠Fe−X−O[f]	ϕ_{Im}[f,g]	ref
Five-Coordinate Complexes								
[Fe(OEP)(NO)]$^+$	0.29	1.994(1)	1.644(3)	1.112(4)		176.9(3)		26
[Fe(OEP)(NO)]$^+$	0.32	1.994(5)	1.6528(13)	1.140(2)		173.19(13)		25
[Fe(OEP)(CO)]	0.20	1.988(2)	1.7140(11)	1.1463(12)		177.20(8)		63
Six-Coordinate Complexes								
[Fe(OEP)(2-MeHIm)(NO)]$^+$	−0.01	1.997(5)	1.641(2)	1.133(3)	2.028(2)	176.6(2)	26.3	this work
[Fe(OEP)(2-MeHIm)(NO)]$^+$(**pla**)	−0.02	2.014(8)	1.649(2)	1.132(3)	2.053(2)	175.6(2)	17.4	48
[Fe(OEP)(2-MeHIm)(NO)]$^+$(**ruf**)	0.03	2.003(7)	1.648(2)	1.139(2)	2.032(2)	177.4(2)	30.2	48
[Fe(OEP)(1-MeIm)(NO)]$^+$	0.02	2.003(5)	1.6465(17)	1.135(2)	1.9889(16)	177.28(17)	31.3	27
[Fe(OETPP)(1-MeIm)(NO)]$^+$	0.09	1.990(9)	1.650(2)	1.130(3)	1.983(2)	177.0(3)	14.6	18
[Fe(OEP)(1-MeIm)(CO)]	0.02	2.010(4)	1.7733(12)	1.1413(15)	2.0544(9)	175.67(11)	NA[h]	64
[Fe(TPP)(1-MeIm)(CO)]	0.02	2.005(6)	1.7600(17)	1.139(2)	2.0503(14)	177.03(15)	30.8	65
[Fe(TPP)(2-MeHIm)(CO)]	−0.01	1.9880(12)	1.7410(14)	1.1488(17)	2.1018(12)	175.96(13)	42.1	65
[Fe(TPP)(1,2-Me_2Im)(CO)]	0.04	1.9853(10)	1.7537(15)	1.1408(19)	2.0779(11)	175.95(14)	43	65
[Fe(β-PocPivP)(1,2-$Me_2$1m)(CO)]	0.00	1.973(8)	1.768(7)	1.148(7)	2.079(5)	172.5(6)	NA[h]	66

[a]Estimated standard deviations are given in parentheses. [b]Displacement of iron atom from the 24-atom mean plane, a positive value is toward the X−O (X = N, C) ligand side. [c]Value in angstroms. [d]Average value in angstroms. [e]X = N or C. [f]Value in degrees. [g]Dihedral angle between imidazole plane and the plane of closest N_p−Fe−N_{ax}. [h]Value not available.

dx.doi.org/10.1021/ja5105766 | J. Am. Chem. Soc. 2014, 136, 18100−18110

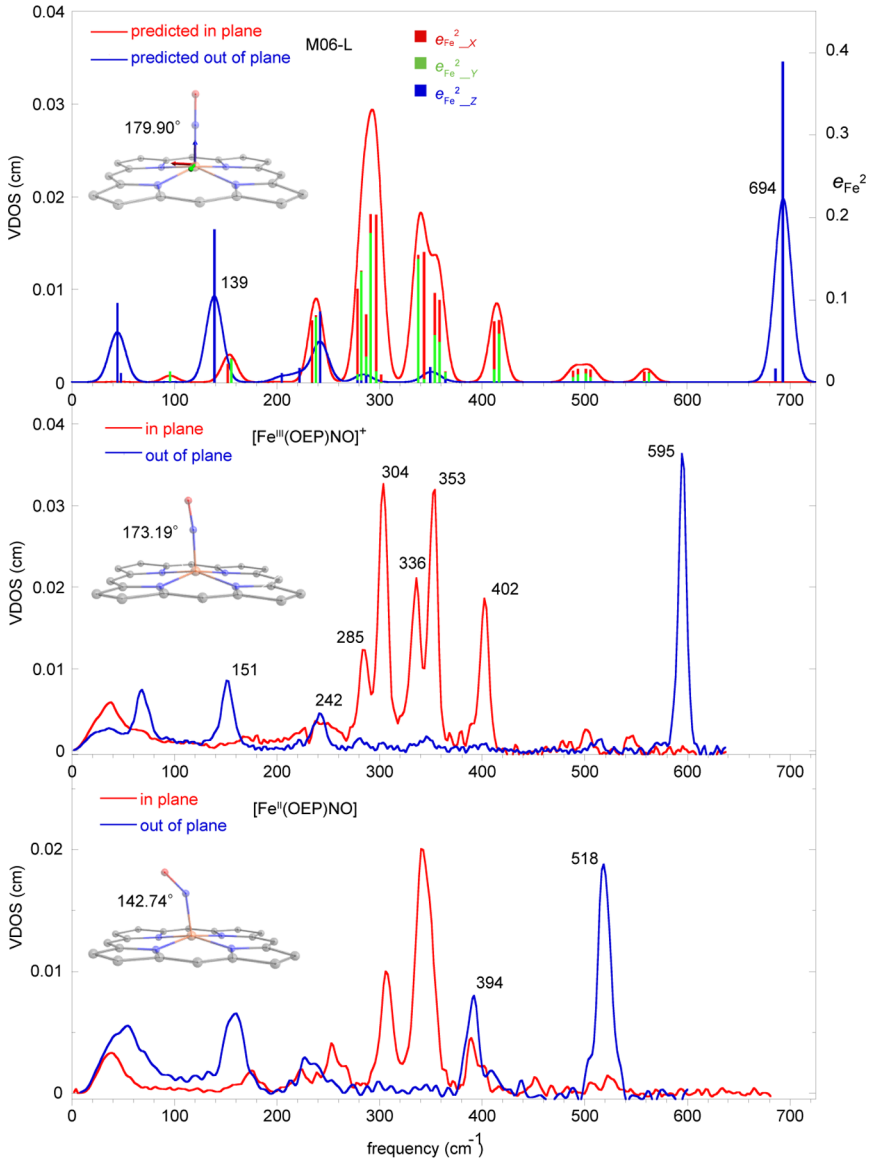

Figure 4. Plots relating to the vibrational spectra of [Fe(OEP)(NO)]$^{+/0}$. The top panel displays the predicted vibrational density of states from an M06-L calculation for [Fe(OEP)(NO)]$^+$. The middle panel shows the experimental VDOS for the in-plane and out-of-plane measurements for [Fe(OEP)(NO)]$^+$. The bottom panel gives the same experimental results for [Fe(OEP)(NO)]; figure data were abstracted from refs 42 and 68.

bonds in the six-coordinate {FeNO}^{6} species are very strong: not only is there no structural trans effect, but the Fe−NO bond is unaffected by the change in coordination number. All species listed in Table 1 have coordination group distances appropriate for a low-spin state for iron.[62]

NRVS Data. The oriented crystal spectra for both the five- and the six-coordinate {FeNO}^{6} derivatives yield clear assignments of the FeNO stretching (out-of-plane) and bending modes (in-plane); compare Figures 3 and 4 (middle panel). These data show how the change in coordination number leads to frequency shifts for these two modes and allows comparison to other known heme systems with diatomic ligands. For the {FeNO}^{6} derivative, [Fe(OEP)(NO)]$^+$, the experimental NRVS value for the Fe−NO stretch is 595 cm^{-1}, and the experimental value for the Fe−N−O bend is 402 cm^{-1}. This pattern, where the stretch is observed at higher frequency than the bend, follows that observed for [Fe(OEP)(CO)][67] (573 and 505 cm^{-1}) and the {FeNO}^{7} derivatives [Fe(OEP)(NO)][42] (517 and 394 cm^{-1}) and [Fe(DPIX)(NO)][68] (528 and 399 cm^{-1}). Frequencies for the six-coordinate species are a bit more nuanced. The frequency patterns for the six-coordinate analogs of CO's[69] and {FeNO}^{7} NO's[70−72] are reversed with the bend now found at higher frequency than the stretch. Thus, the observed bend is 582 cm^{-1} and the stretch is 499/513 cm^{-1} for [Fe(OEP)(1-MeIm)(CO)],[69] and the bend is 559 cm^{-1} and the stretch is 433 cm^{-1} for [Fe(TpFPP)(1-MeIm)(NO)].[71] Again, in these cases, the value of the stretching mode decreases whereas the value of the bending mode increases. However, for [Fe(OEP)(2-MeHIm)(NO)]$^+$, the observed Fe−NO stretch remains high at 600 cm^{-1}, whereas the two near-degenerate bending modes increase to the observed values of 574 and 580 cm^{-1}. Thus, with the very similar frequencies for both the stretching and the bending modes, the pattern in six-coordinate {FeNO}^{6} species is quite distinct from other six-coordinate diatomics. The close similarity of the Fe−NO stretch in the two coordination numbers undoubtedly reflects that the axial Fe−N(NO) bond distances are unchanged.

dx.doi.org/10.1021/ja5105766 | J. Am. Chem. Soc. 2014, 136, 18100−18110

The bottom two panels of Figure 4 compare the NRVS spectra of [Fe(OEP)(NO)]$^+$ and [Fe(OEP)(NO)].[42] The Fe−NO stretch in the cation is found to be 78 cm^{-1} higher, at 595 cm^{-1} as compared to 517 cm^{-1}, consistent with the ∼0.1 Å decrease in the Fe−NO bond distances.[25,26,73−79] The purely in-plane bending mode of iron at 402 cm^{-1} in [Fe(OEP)(NO)]$^+$ contrasts with the in-plane and out-of-plane components of the bend in [Fe(OEP)(NO)] along with a small decrease in the observed frequency.

We have also carried out a series of DFT calculations to aid in understanding the complete vibrational spectra. For [Fe(OEP)(2-MeHIm)(NO)]$^+$, three sets of DFT calculations based on the use of functionals M06-L, BP86, and B3LYP were completed. All predictions gave resolved bending and stretching modes with the stretching mode always at higher frequency; the best match of the predicted spectra to the total observed spectra was given by the M06-L calculations, and those will be used here. Results of the other predictions are given in the Supporting Information. Consistent with the experimental spectra, there are three main spectral regions to be considered. The peaks in the ∼570−610 cm^{-1} region are associated with the axial NO ligand. As has been commonly observed, the vibrational prediction for the axial stretch is at higher frequency than that observed.[60,80−82] In the lower frequency regions, there are intense peaks in two distinct regions. Those between ∼300−370 cm^{-1} are mostly associated with in-plane iron motions, whereas those in the region of ∼200−280 cm^{-1} are dominated by out-of-plane iron motion. There is some in-plane/out-of-plane overlap in the 240−280 cm^{-1} range. The complete predicted spectrum is illustrated in Figure 5.

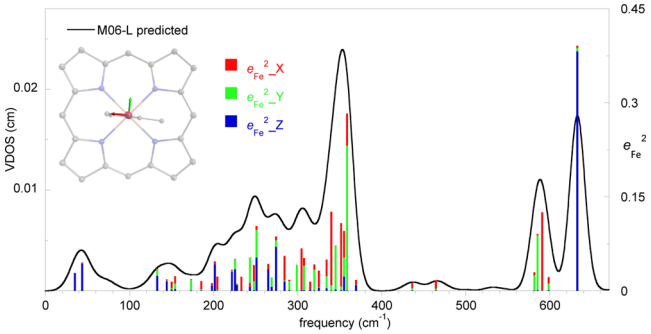

Figure 5. Complete M06-L predicted spectrum of [Fe(OEP)(2-MeHIm)(NO)]$^+$ further showing (as e^2 values, bars) the directional components in the three orthogonal directions.

DFT calculations for [Fe(OEP)(NO)]$^+$ were carried out with the M06-L and BP86 functionals. Again, the M06-L functional gave better matches to the observed spectra. (See top panel of Figure 4.) The predictions are in general accord with the experimental data. The predicted bending mode frequencies are found substantially below the stretch as observed in the single-crystal data. These two bending modes (at 414.3 and 414.4 cm^{-1}) are shown in Figure S8 (Supporting Information). This is in distinct contrast to the in-plane modes of [Fe(OEP)(2-MeHIm)(NO)]$^+$ where the planar axial imidazole removes the x and y degeneracy.

Thus, the two major orthogonal bending modes predicted at 585 and 591 cm^{-1} are localized perpendicular or parallel to the imidazole plane, respectively (Figure 5). These correspond to the observed peaks at 574 and 580 cm^{-1}; the relative directionality and frequency orderings are preserved. MOLEKEL depictions of the two modes are given in Figure 6. As can

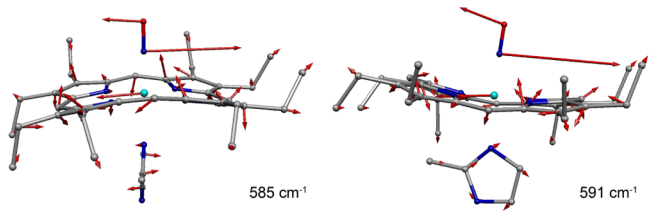

Figure 6. DFT (M06-L) predicted Fe−NO bending modes of [Fe(OEP)(2-MeHIm)(NO)]$^+$ at 585 and 591 cm^{-1}.

be seen, the motions of the imidazole are also in the direction of the bend, thus ring rotation for the 591 cm^{-1} mode and motion perpendicular to the ring plane in the 585 cm^{-1} mode. Two minor in-plane peaks are also predicted (Figure 5); these may explain the shoulders seen at higher frequencies in both the in-plane x and the in-plane y spectra (Figure 3). It is to be noted however that the in-plane x shoulder is more intense than the DFT predictions would suggest.

For both species, there are a number of in-plane vibrations below ∼370 cm^{-1}. These modes are generally porphyrin vibrations, especially ν_{49}, ν_{50}, and ν_{53}. Both the five- and the six-coordinate complexes exhibit four relatively intense vibrations in the 338−360 cm^{-1} region. These frequencies are those expected for the low-spin state. The two species do differ in the predicted motion of iron. For [Fe(OEP)(2-MeHIm)(NO)]$^+$, both near-degenerate pairs of vibrations have the iron motion approximately parallel or perpendicular to the axial imidazole plane. We also note that the highest frequency vibration is observed and predicted to have more intensity than the others. See Figure 7 for MOLEKEL depictions of these modes. [Fe(OEP)(NO)]$^+$, on the other hand, has the two pairs of iron motions in this region, one set along Fe−N$_p$ bonds and a second set halfway between Fe−N$_p$ bonds. The observed

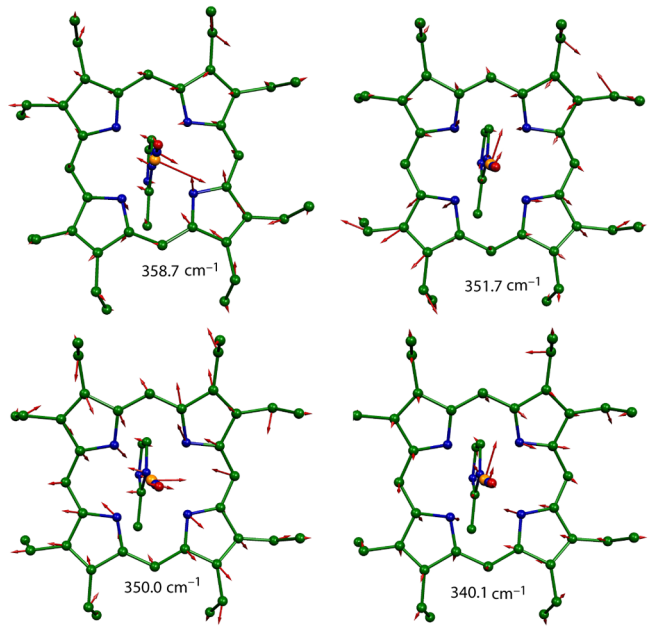

Figure 7. MOLEKEL depictions of the four highest frequency in-plane modes of [Fe(OEP)(2-MeHIm)(NO)]$^+$.

dx.doi.org/10.1021/ja5105766 | J. Am. Chem. Soc. 2014, 136, 18100−18110

maxima are found at 336 and 353 cm^{-1}. These are illustrated in the MOLEKEL depictions found in the Supporting Information (Figure S9). $[Fe(OEP)(NO)]^+$ also has a second group of in-plane vibrations centered around ~295 cm^{-1}. The predicted *x* and *y* components are essentially equivalent, consistent with little or no anisotropy in the porphyrin plane. The differences in the in-plane iron motion in the two complexes probably reflect differences in the out-of-plane displacements of iron that lead to differing amounts of mixing with the ligand vibrations.

At lower frequencies, the in-plane iron vibrations of $[Fe(OEP)(2\text{-}MeHIm)(NO)]^+$ are distributed over a large range of modes mixed with ligand vibrations and not well resolved in the experimental spectra. For $[Fe(OEP)(NO)]^+$, on the other hand, the in-plane modes are less mixed and are predicted to occur over a smaller number of frequencies that are resolved both experimentally (peaks at 285 and 304 cm^{-1}) and theoretically. These are shown in Figure S10 of the Supporting Information.

The highest frequency peak in the *z* direction spectra of $[Fe(OEP)(2\text{-}MeHIm)(NO)]^+$ is observed at 600 cm^{-1}, which is clearly higher than the bending mode frequencies already described. The prediction of a peak 33 cm^{-1} higher than observed is not unexpected as the axial ligand frequencies have always been the most difficult prediction for the DFT calculations.[80] The character of the M06-L prediction for $[Fe(OEP)(2\text{-}MeHIm)(NO)]^+$ is shown in Figure 8. Thus, the Fe–NO stretch is always observed and predicted at higher frequency than the bend. We believe that the stretch/bend assignments made[37] for $[Fe(TPP)(1\text{-}MeIm)(NO)]^+$ should be emended to have the stretch at higher frequency than the bend.[83] Although we believe that the assignments by Lehnert et al. should have the stretch at higher frequency than the bends, their conclusions will be similar for either choice of assignment. Incorrect assignments might, however, cause difficulties in creating possible spectral correlations. The analogous Fe–NO stretch in $[Fe(OEP)(NO)]^+$ is seen at 595 cm^{-1}, whereas the predicted position at 694 cm^{-1} shows a much large deviation. We have noted that the axial stretch prediction discrepancies are frequently larger in the five-coordinate systems.

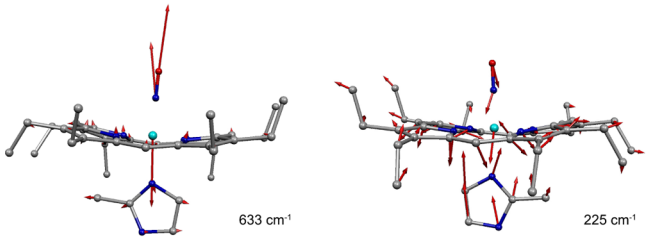

Figure 8. DFT (M06-L) predicted Fe–NO stretch mode (633 cm^{-1}) and Fe–Im stretch mode (225 cm^{-1}) of $[Fe(OEP)(2\text{-}MeHIm)(NO)]^+$.

Other axial iron vibrations are those of the doming and inverse doming modes. For the five-coordinate species, the inverse doming mode is predicted at 242 cm^{-1} and the doming mode at 139 cm^{-1}. Observed values are 242 and 151 cm^{-1}, respectively. Values for the six-coordinate species are 144 cm^{-1} for the doming mode, and the observed value is 152 cm^{-1}. Modes involving reverse doming in the six-coordinate species are strongly mixed with other modes, but the predicted character of the frequencies at 221 and 274 cm^{-1} does show this character.

Probably the most interesting axial vibration is that of iron to the proximal imidazole. In five-coordinate iron(II) derivatives, the Fe–Im stretch is readily observed by resonance Raman spectroscopy and has been used extensively for protein and small-molecule characterization. A range of frequencies for histidine-ligated proteins is observed (~200–256 cm^{-1})[84−93] that are correlated with the strength of the Fe–Im bond. Factors that are known to influence the bond strength include whether or not the histidine N_δ is hydrogen bonded.[94] The formation of an imidazolate leads to the highest frequencies.[95] The relative ligand orientation may also play a role.[96,97]

Unfortunately, for six-coordinate species, bands associated with the Fe–Im stretch are typically not observed in resonance Raman experiments, so that very little information has been available. Nuclear resonance vibrational spectroscopy provides experimental information on all iron vibrations and thus provides direct quantitative information. However, the

Table 2. Fe–Im Stretch Vibrations (NRVS and Calculation) and X-ray Determined Fe–N_{Im} Bond Distances for [Fe(Porph)(RIm)(XO)] Complexes (X = N, C, or O)

complex	method		ν_{Fe-Im} [a]		Fe–N_{Im} [b]	ref
		Fe(III)				
$[Fe(OEP)(2\text{-}MeHIm)(NO)]^+$	SC NRVS[c]	238	230	222	2.028(2)	this work
	DFT(M06-L)	225	222	201		this work
		Fe(II)				
[Fe(TPP)(1-MeIm)(CO)]	SC NRVS[c]	225	172		2.0503(14)	65, 69
	DFT(B3LYP)	214	182			69
[Fe(TPP)(1-MeIm)(NO)]	SC NRVS[c]	149	175		2.173(2)	70, 98
	QCC-NCA	151	176			99
tri-[Fe(T*p*FPP)(1-MeIm)(NO)]	SC NRVS[c]	140	167		2.1689(9)	71
mono-[Fe(T*p*FPP)(1-MeIm)(NO)]	SC NRVS[c]	153	177		2.1312(11)	71
	DFT(B3LYP)	147	166			71
$[Fe(TpivPP)(1\text{-}EtIm)(O_2)]$	SC NRVS[c]	196	174	134	2.043(3)	100, 101
	DFT(B3LYP)	195	169	143		100
$[Fe(TpivPP)(2\text{-}MeHIm)(O_2)]$	S-C NRVS[c]	187	175	130	2.091(5)	100, 101
$[Fe(TpivPP)(1\text{-}MeIm)(O_2)]$	powder NRVS	205	175	136		100

[a]The frequency (in cm^{-1}) with the motion that most closely resembles that of the classical Fe–Im stretch is given first. [b]Value in angstroms. [c]Obtained from single-crystal NRVS experiment.

dx.doi.org/10.1021/ja5105766 | J. Am. Chem. Soc. 2014, 136, 18100−18110

appearance of more than one predicted mode with simultaneous iron and imidazole motion in this system as well as in previously studied six-coordinate O_2, CO, and {FeNO}^{7} hemes leads to the difficult question of which frequency provides the most accurate experimental description of the Fe−Im bond. We have used the following procedure for this. We examine the predicted character of each calculated frequency and choose the one that best resembles the classical Fe−Im stretch. This "classical" Fe−Im vibration for [Fe(OEP)(2-MeHIm)(NO)]$^+$ is illustrated in Figure 8 (225 cm^{-1}). The similarity of this mode to others previously published can be seen in the simulations displayed in Figure 9 of ref 69 for [Fe(TPP)(1-MeIm)(CO)] and Figure S9 of ref 100 for [Fe(TpivPP)(1-EtIm)(O_2)]. We then match the predicted and experimental frequencies to choose the best experimental value for the stretch for all available compounds.

The experimental Fe−Im stretch frequencies are given in Table 2 that also gives the experimental value of the trans Fe−N(Im) bond distance. There are a total of seven distinct species for which both the Fe−Im stretch and the Fe−N(Im) bond distance have now been experimentally determined. Figure 9

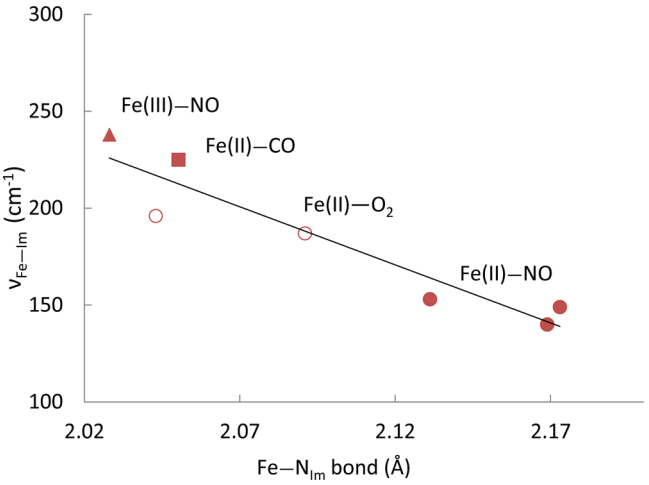

Figure 9. Correlation between Fe−N_{Im} bond distances and Fe−Im stretch frequencies (ν_{Fe-Im}) of six-coordinate [Fe(Porph)(RIm)(XO)] (X = N, C, O) complexes. ▲, [Fe(OEP)(2-MeHIm)(NO)]$^+$; ■, [Fe(TPP)(1-MeIm)(CO)]; ○, [Fe(TpivPP)(2-MeHIm)(O_2)] and [Fe(TpivPP)(1-MeIm)(O_2)]; ●, [Fe(TPP)(1-MeIm)(NO)], tri-[Fe(T*p*FPP)(1-MeIm)(NO)], and mono-[Fe(T*p*FPP)(1-MeIm)(NO)]. Literature citations are given in Table 2.

plots the relationship between the two. The correlation between the two is clearly evident and extends over a large range of distances and frequencies. The strong correlation displayed may strike some as self-evident, but we note that this is the first time that such experimental data have been marshalled for a possible correlation. The correlation clearly can be extended for the characterization of systems in which only the vibrational data or the structural data are available. Note that all of the Fe−Im stretching frequencies listed in Table 2 are based on oriented single-crystal NRVS measurements.

In our view, the description of the electronic state of the six-coordinate {FeNO}^{6} species remains enigmatic. The isoelectronic character of {FeNO}^{6} and {FeCO}^{6} species has often been expressed, with the implied expectation of strong similarities; however, our DFT calculations for [Fe(OEP)(2-MeHIm)(NO)]$^+$ and [Fe(OEP)(2-MeHIm)(CO)] show large differences in the relative energies of equivalent MO's. Similar results have been obtained previously.[102]

The IR and NRVS vibrational data for [Fe(Porph)(R−Im)(NO)]$^+$ species are consistent with calculations that predict a formal oxidation state description as Fe(II)(NO$^+$). The observed Mössbauer spectra with the very small values for the isomer shift are highly unusual for an iron(II) state; rather they are similar to those observed for iron(IV). Yet calculations of Neese suggest that this is a bonding effect that results from the extremely strong π-bonding of an NO$^+$ ligand.[103]

The observed very strong Fe−N(NO) bond, yet the facile loss of NO in [Fe(Porph)(R−Im)(NO)]$^+$ species, has puzzled many investigators. Recent calculations of Lehnert and co-workers have attempted to explain this perhaps paradoxical behavior. Praneeth et al.'s calculations[37] predict the ground-state structure of six-coordinate [Fe(Porph)(R−Im)(NO)]$^+$ species as Fe(II)(NO$^+$), with its very short axial Fe−N(NO) bond distance. They further posit the existence of high- and low-spin Fe(III)−NO(radical) states that are low-lying states lying within a few kcal/mol of the ground state. The first excited state could be within 1.0−1.3 kcal/mol of the ground state.[37] They propose that it is these states, with weaker Fe−N(NO) and N−O bond strengths, that lead to the facile loss of NO.

Although this suggestion has some reasonable features, we expect that the existence of such close-lying states would lead to substantial *T*-dependent Mössbauer quadrupole splitting values as has been seen in the dioxygen complexes of hemoglobin and myoglobin.[32,104] If the separation of ground and excited states was 1.3 kcal/mol, the excited state would be populated by ∼15%, sufficient to have temperature effects on the quadrupole splitting value. Although the experimentally available Mössbauer data are limited,[25] the expected temperature dependence of the quadrupole splitting is not observed, thus casting some doubt on the suggestion of close lying states. However, a significantly higher energy difference has been given based on CASSCF or TD-DFT calculations.[105] Further experimental and theoretical work on these challenging compounds is clearly warranted.

■ SUMMARY

Oriented single-crystal NRVS studies for [Fe(OEP)(NO)]$^+$ and [Fe(OEP)(2-MeHIm)(NO)]$^+$ provide unequivocal assignments for the Fe−N−O stretching and bending modes for both. The differing pattern of stretch and bend as a function of coordination number for the {FeNO}^{6} derivatives is noted and compared to the patterns previously observed for the related CO and {FeNO}^{7} hemes. The use of NRVS methods allows the observation and assignments of the several out-of-plane frequencies that are typically not observed by other spectroscopic methods. In particular, the availability of the previously unobserved Fe−Im stretching frequency and structural data for seven distinct O_2, NO, and CO species establishes a correlation between the Fe−Im stretch and the Fe−N_{Im} bond distance.

■ ASSOCIATED CONTENT

Ⓢ Supporting Information

Tables giving complete crystallographic information for [Fe(OEP)(2-MeHIm)(NO)]ClO_4 and e^2_{Fe} values >0.01 for [Fe(OEP)(NO)]$^+$, and [Fe(OEP)(2-MeHIm)(NO)]$^+$ including complete directional values. A crystallographic information

dx.doi.org/10.1021/ja5105766 | J. Am. Chem. Soc. 2014, 136, 18100−18110

file for [Fe(OEP)(2-MeHIm)(NO)]ClO_4. Figure S1 showing the unit cell and the parallel porphyrin planes. Figures S2−S5 displaying the BP86 and B3LYP predicted VDOS and directional characteristics for $[Fe(OEP)(2\text{-}MeHIm)(NO)]^+$. Figures S6 and S7 showing the comparison of the experimental and predicted VDOS and predicted kinetic energy distributions in the z direction. Figure S8 showing the two orthogonal bending modes in $[Fe(OEP)(NO)]^+$, Figure S9 showing the MOLEKEL depictions of the four predicted in-plane modes around 356 cm^{-1}, and Figure S10 showing the five highest intensity in-plane modes in the 280−300 cm^{-1} region. This material is available free of charge via the Internet at http://pubs.acs.org.

AUTHOR INFORMATION

Corresponding Authors

jfli@ucas.ac.cn
jtsage@neu.edu
scheidt.1@nd.edu

Notes

The authors declare no competing financial interest.

ACKNOWLEDGMENTS

Research reported in this publication was supported by a CAS Hundred Talent Program and National Natural Science Foundation of China (Grant no. 21371167) to J.L., the National Institutes of Health under Grant GM-38401 to W.R.S., and the National Science Foundation under CHE-1026369 to J.T.S. W.R.S. acknowledges a CAS Professorship for Senior International Scientists. Use of the Advanced Photon Source, an Office of Science User Facility operated for the U.S. Department of Energy (DOE) Office of Science by Argonne National Laboratory, was supported by the U.S. DOE under contract no. DE-AC02-06CH11357.

REFERENCES

(1) Ghosh, A., Ed. *The Smallest Biomolecules: Diatomics and Their Interactions with Heme Protein*; Elsevier: Amsterdam, 2008.
(2) Rodgers, K. R. *Curr. Opin. Chem. Biol.* **1999**, *3*, 158.
(3) Ma, X.; Sayed, N.; Bueve, A.; van den Akker, F. *EMBO J.* **2007**, *26*, 578.
(4) Nioche, P.; Berka, V.; Vipond, J.; Minton, N.; Tsai, A.; Raman, C. S. *Science* **2004**, *306*, 1550.
(5) Erbil, W. K.; Price, M. S.; Wemmer, D. E.; Marletta, M. A. *Proc. Natl. Acad. Sci. U.S.A.* **2009**, *106*, 19753.
(6) Richter-Addo, G. B., Legzdins, P., Burstyn, J., Eds. *Chem. Rev.* **2002**, *102*, 857−1270.
(7) The $\{FeNO\}^n$ notation is that of Enemark and Feltham,[8] where n is the number of d electrons plus the number of electrons in the π^* orbitals of NO. The notation is designed to strongly emphasize the highly covalent nature of the triatomic FeNO unit.
(8) Enemark, J. H.; Feltham, R. D. *Coord. Chem. Rev.* **1974**, *13*, 339.
(9) Ignarro, L. J. *Nitric Oxide: Biology and Pathobiology*, 2nd ed.; Elsevier: Amsterdam, 2010.
(10) Kots, A. Y.; Martin, E.; Sharina, I. G.; Murad, F. In *Handbook of Experimental Pharmacology*; Schmidt, H. H., Hofmann, F., Stasch, J.-P., Eds.; Springer-Verlag: Berlin, 2009; pp 1−14.
(11) Russwurm, M.; Koesling, D. *EMBO J.* **2004**, *23*, 4443.
(12) Moncada, S.; Palmer, R. M. J.; Higgs, E. A. *Pharmacol. Rev.* **1991**, *43*, 109.
(13) Snyder, S. H. *Science* **1992**, *257*, 494.
(14) Butler, A. R.; Williams, D. L. H. *Chem. Soc. Rev.* **1993**, 233.
(15) Stamler, J. S.; Singel, D. J.; Loscalzo, J. *Science* **1992**, *258*, 1898.
(16) Hughes, M. N. *Biochim. Biophys. Acta* **1999**, *1411*, 263.
(17) Cooper, C. E. *Biochim. Biophys. Acta* **1999**, *1411*, 290.
(18) Drapier, J.-C.; Pellat, C.; Henry, Y. *J. Biol. Chem.* **1991**, *266*, 10162.
(19) Stadler, J.; Bergonia, H. A.; Di Silvio, M.; Sweetland, M. A.; Billiar, T. R.; Simmons, R. L.; Lancaster, J. R. *Arch. Biochem. Biophys.* **1993**, *302*, 4.
(20) Terenzi, F.; Diaz-Guerra, M. J. M.; Casado, M.; Hortelano, S.; Leoni, S.; Bosca, L. *J. Biol. Chem.* **1995**, *270*, 6017.
(21) Lehnert, N.; Scheidt, W. R.; Wolf, M. W. *Struct. Bonding (Berlin)* **2014**, *154*, 155.
(22) Walker, F. A. *J. Inorg. Biochem.* **2005**, *99*, 216.
(23) Fülöp, V.; Moir, J. W. B.; Ferguson, S. J.; Hajdu, J. *Cell* **1995**, *81*, 369.
(24) Wasser, I. M.; de Vries, S.; Moenne-Loccoz, P.; Schroder, I.; Karlin, K. D. *Chem. Rev.* **2002**, *102*, 1201.
(25) Ellison, M. K.; Schulz, C. E.; Scheidt, W. R. *Inorg. Chem.* **2000**, *39*, 5102.
(26) Scheidt, W. R.; Lee, Y. J.; Hatano, K. *J. Am. Chem. Soc.* **1984**, *106*, 3191.
(27) Ellison, M. K.; Scheidt, W. R. *J. Am. Chem. Soc.* **1999**, *121*, 5210.
(28) Abbreviations: R−Im, generalized imidazole in small-molecule systems and the histidine ligand in proteins; Porph, dianion of a generalized porphyrin; OEP, dianion of octaethylporphyrin; TPP, dianion of tetraphenylporphyrin; TpFPP, dianion of tetra-*p*-fluorophenylporphyrin; TpivPP, dianion of picket fence porphyrin; DPIX, dianion of deuteroporphyrin IX dimethylester; OETPP, dianion of octaethyltetraphenylporphyrin; β-PocPivP, pocket porphyrin dianion; 2-MeHIm, 2-methylimidazole; NRVS, nuclear resonance vibrational spectroscopy; VDOS, vibrational density of states.
(29) Ozawa, S.; Sakamoto, E.; Ichikawa, T.; Watanabe, Y.; Morishima, I. *Inorg. Chem.* **1995**, *34*, 6362.
(30) Mu, X. H.; Kadish, K. M. *Inorg. Chem.* **1988**, *27*, 4720.
(31) Fujita, E.; Fajer, J. *J. Am. Chem. Soc.* **1983**, *105*, 6743.
(32) Debrunner, P. G. In *Iron Porphyrins*; Lever, A. B. P., Gray, H. B., Eds.; VCH Publishers Inc.: New York, 1983; Part 3, Chapter 2.
(33) Pauling, L.; Coryell, C. D. *Proc. Natl. Acad. Sci. U.S.A.* **1936**, *22*, 210.
(34) Chen, H.; Ikeda-Saito, M.; Shaik, S. *J. Am. Chem. Soc.* **2008**, *130*, 14778. This paper provides a long introduction to the various models.
(35) Benko, B.; Yu, N. T. *Proc. Natl. Acad. Sci. U.S.A.* **1983**, *80*, 7042.
(36) Soldatova, A. V.; Ibrahim, M.; Olson, J. S.; Czernuszewicz, R. S.; Spiro, T. G. *J. Am. Chem. Soc.* **2010**, *132*, 4614.
(37) Praneeth, V. K. K.; Paulat, F.; Berto, T. C.; DeBeer George, S.; Naether, C.; Sulok, C. D.; Lehnert, N. *J. Am. Chem. Soc.* **2008**, *132*, 15288.
(38) Moeser, B.; Janoschka, A.; Wolny, J. A.; Paulsen, H.; Filippov, I.; Berry, R. E.; Zhang, H.; Chumakov, A. I.; Walker, F. A.; Schünemann, V. *J. Am. Chem. Soc.* **2012**, *134*, 4216.
(39) Sage, J. T.; Paxson, C.; Wyllie, G. R. A.; Sturhahn, W.; Durbin, S. M.; Champion, P. M.; Alp, E. E.; Scheidt, W. R. *J. Phys.: Condens. Matter* **2001**, *13*, 7707.
(40) Scheidt, W. R.; Durbin, S. M.; Sage, J. T. *J. Inorg. Biochem.* **2005**, *99*, 60.
(41) Zeng, W.; Silvernail, N. J.; Scheidt, W. R.; Sage, J. T. Nuclear Resonance Vibrational Spectroscopy (NRVS). In *Applications of Physical Methods to Inorganic and Bioinorganic Chemistry*; Scott, R. A., Lukehart, C. M., Eds.; John Wiley and Sons, Ltd.: Chichester, UK, 2007; pp 401−421.
(42) Pavlik, J. W.; Barabanchikov, A.; Oliver, A. G.; Alp, E. E.; Sturhahn, W.; Zhao, J.; Sage, J. T.; Scheidt, W. R. *Angew. Chem., Int. Ed.* **2010**, *49*, 4400.
(43) Zhu, L.; Sage, J. T.; Champion, P. M. *Science* **1994**, *266*, 629.
(44) Milgram, B. C.; Eskildsen, K.; Richter, S. M.; Scheidt, W. R.; Scheidt, K. A. *J. Org. Chem.* **2007**, *72*, 3941.
(45) Dodd, R. E.; Robinson, P. L. *Experimental Inorganic Chemistry*; Elsevier: New York, 1957; p 253.
(46) Landergren, M.; Baltzer, L. *Inorg. Chem.* **1990**, *29*, 556.
(47) Scheidt, W. R.; Cohen, I. A.; Kastner, M. E. *Biochemistry* **1979**, *18*, 3546.

(48) Ellison, M. K.; Schulz, C. E.; Scheidt, W. R. *J. Am. Chem. Soc.* **2002**, *124*, 13833.
(49) Scheidt, W. R.; Geiger, D. K.; Lee, Y. J.; Reed, C. A.; Lang, G. *J. Am. Chem. Soc.* **1985**, *107*, 5693.
(50) Sheldrick, G. M. *Program for Empirical Absorption Correction of Area Detector Data*; Universität Göttingen: Germany, 1996.
(51) Sheldrick, G. M. *Acta Crystallogr., Sect. A* **2008**, *A64*, 112.
(52) $R_1 = \sum||F_o| - |F_c||/\sum|F_o|$ and $wR_2 = \{\sum[w(F_o^2 - F_c^2)^2]/\sum[wF_o^4]\}^{1/2}$. The conventional *R*-factors R_1 are based on *F*, with *F* set to zero for negative F^2. The criterion of $F^2 > 2\sigma(F^2)$ was used only for calculating R_1. *R*-factors based on F^2 (wR_2) are statistically about twice as large as those based on *F*, and *R*-factors based on all data will be even larger.
(53) (a) Macrae, C. F.; Edgington, P. R.; McCabe, P.; Pidcock, E.; Shields, G. P.; Taylor, R.; Towler, M.; van de Streek, J. *J. Appl. Crystallogr.* **2006**, *39*, 453. (b) Bruno, I. J.; Cole, J. C.; Edgington, P. R.; Kessler, M. K.; Macrae, C. F.; McCabe, P.; Pearson, J.; Taylor, R. *Acta Crystallogr.* **2002**, *B58*, 389. (c) Taylor, R.; Macrae, C. F. *Acta Crystallogr.* **2001**, *B57*, 815.
(54) Toellner, T. S. *Hyperfine Interact.* **2000**, *125*, 3.
(55) Sturhahn, W.; Toellner, T. S.; Alp, E. E.; Zhang, X. W.; Ando, M.; Yoda, Y.; Kikuta, S.; Seto, M.; Kimball, C. W.; Dabrowski, B. *Phys. Rev. Lett.* **1995**, *74*, 3832.
(56) Frisch, M. J.; Trucks, G. W.; Schlegel, H. B.; Scuseria, G. E.; Robb, M. A.; Cheeseman, J. R.; Scalmani,G.; Barone, V.; Mennucci, B.; Petersson, G. A.; Nakatsuji, H.; Caricato, M.; Li, X.; Hratchian, H. P.; Izmaylov, A. F.; Bloino, J.; Zheng, G.; Sonnenberg, J. L.; Hada, M.; Ehara, M.; Toyota, K.; Fukuda, R.; Hasegawa, J.; Ishida, M.; Nakajima,T..; Honda, Y.; Kitao, O.; Nakai, H.; Vreven, T.; Montgomery, J. A., Jr.; Peralta, J. E.; Ogliaro, F. ; Bearpark, M.; Heyd, J. J.; Brothers, E.; Kudin, K. N.; Staroverov, V. N.; Kobayashi, R.; Normand, J.; Raghavachari, K.; Rendell, A.; Burant, J. C.; Iyengar, S. S.; Tomasi, J.; Cossi, M.; Rega, N.; Millam, J. M.; Klene, M.; Knox, J. E.; Cross, J. B.; Bakken, V.; Adamo, C.; Jaramillo, J.; Gomperts, R.; Stratmann, R. E.; Yazyev, O.; Austin, A. J.; Cammi, R.; Pomelli, C.; Ochterski, J. W.; Martin, R. L.; Morokuma, K.; Zakrzewski, V. G.; Voth, G. A.; Salvador, P.; Dannenberg, J. J.; Dapprich, S.; Daniels, A. D.; Farkas, O.; Foresman, J. B.; Ortiz, J. V.; Cioslowski, J.; Fox, D. J. *Gaussian 09*, revision A.02; Gaussian, Inc.: Wallingford, CT, 2009.
(57) (a) Becke, A. D. *Phys. Rev.* **1988**, *A38*, 3098. (b) Perdew, J. P. *Phys. Rev.* **1986**, *B33*, 8822.
(58) Zhao, Y.; Truhlar, D. G. *J. Chem. Phys.* **2006**, *125*, 194101.
(59) Schäfer, A.; Horn, H.; Ahlrichs, R. *J. Chem. Phys.* **1992**, *97*, 2571.
(60) Peng, Q.; Pavlik, J. W.; Scheidt, W. R.; Wiest, O. *J. Chem. Theory Comput.* **2012**, *8*, 214.
(61) The definitions of the *x* and *y* in this Article for [Fe(OEP)(2-MeHIm)(NO)]ClO_4 have *x* parallel to the imidazole plane and *y* perpendicular to the imidazole plane. The definition for [Fe(OEP)(NO)]ClO_4 has *x* and *y* along the Fe−N_p directions.
(62) Scheidt, W. R.; Reed, C. A. *Chem. Rev.* **1981**, *81*, 543.
(63) Silvernail, N. J.; Noll, B. C.; Schulz, C. E.; Scheidt, W. R. *Inorg. Chem.* **2006**, *45*, 7050.
(64) Silvernail, N. J.; Noll, B. C.; Scheidt, W. R., manuscript in preparation.
(65) Silvernail, N. J.; Roth, A.; Schulz, C. E.; Noll, B. C.; Scheidt, W. R. *J. Am. Chem. Soc.* **2005**, *127*, 14422.
(66) Kim, K.; Fettinger, J. C.; Sessler, J. L.; Cyr, M.; Hugdahl, J.; Collman, J. P.; Ibers, J. A. *J. Am. Chem. Soc.* **1989**, *111*, 403.
(67) Linder, D. P.; Silvernail, N. J.; Barabanschikov, A.; Zhao, J.; Alp, E. E.; Sturhahn, W.; Sage, J. T.; Scheidt, W. R.; Rodgers, K. R. *J. Am. Chem. Soc.* **2014**, *136*, 9818.
(68) Pavlik, J. W.; Peng, Q.; Silvernail, N. J.; Alp, E. E.; Hu, M. Y.; Zhao, J.; Sage, J. T.; Scheidt, W. R. *Inorg. Chem.* **2014**, *53*, 2582.
(69) Leu, B. M.; Silvernail, N. J.; Zgierski, M. Z.; Wyllie, G. R. A.; Ellison, M. K.; Scheidt, W. R.; Zhao, J.; Sturhahn, W.; Alp, E. E.; Sage, J. T. *Biophys. J.* **2007**, *92*, 3764.
(70) Zeng, W.; Silvernail, N. J.; Wharton, D. C.; Georgiev, G. Y.; Leu, B. M.; Scheidt, W. R.; Zhao, J.; Sturhahn, W.; Alp, E. E.; Sage, J. T. *J. Am. Chem. Soc.* **2005**, *127*, 11200.
(71) Silvernail, N. J.; Barabanschikov, A.; Pavlik, J. W.; Noll, B. C.; Zhao, J.; Alp, E. E.; Sturhahn, W.; Sage, J. T.; Scheidt, W. R. *J. Am. Chem. Soc.* **2007**, *129*, 2200.
(72) Paulat, F.; Berto, T. C.; DeBeer George, S.; Goodrich, L.; Praneeth, V. K. K.; Sulok, C. D.; Lehnert, N. *Inorg. Chem.* **2008**, *47*, 11449. Initial assignments of stretch and bend were based on oriented crystal measurements (refs 70 and 71) and confirmed by isotopic labeling.
(73) Scheidt, W. R.; Frisse, M. E. *J. Am. Chem. Soc.* **1975**, *97*, 17.
(74) Ellison, M. K.; Scheidt, W. R. *J. Am. Chem. Soc.* **1997**, *119*, 7404.
(75) Scheidt, W. R.; Duval, H. F.; Neal, T. J.; Ellison, M. K. *J. Am. Chem. Soc.* **2000**, *122*, 4651.
(76) Bohle, D. S.; Debrunner, P.; Fitzgerald, J.; Hansert, B.; Hung, C.-H.; Thompson, A. J. *J. Chem. Soc., Chem. Commun.* **1997**, 91.
(77) Wyllie, G. R. A.; Scheidt, W. R. *Inorg. Chem.* **2003**, *42*, 4259.
(78) Silvernail, N. J.; Olmstead, M. M.; Noll, B. C.; Scheidt, W. R. *Inorg. Chem.* **2009**, *48*, 971.
(79) Wyllie, G. R. A.; Silvernail, N. J.; Oliver, A. G.; Schulz, C. E.; Scheidt, W. R. *Inorg. Chem.* **2014**, *53*, 3763.
(80) Leu, B.; Zgierski, M.; Wyllie, G. R. A.; Scheidt, W. R.; Sturhahn, W.; Alp, E. E.; Durbin, S. M.; Sage, J. T. *J. Am. Chem. Soc.* **2004**, *126*, 4211. In this initial use of DFT for the vibrational predictions of [Fe(OEP)(NO)], we found that some calculations gave predictions of the axial Fe−NO stretch that were much higher than actually observed.
(81) Goodrich, L. E.; Paulat, F.; Praneeth, V. K. K.; Lehnert, N. *Inorg. Chem.* **2010**, *49*, 6293.
(82) Scheidt, W. R.; Barabanschikov, A.; Pavlik, J. W.; Silvernail, N. J.; Sage, J. T. *Inorg. Chem.* **2010**, *49*, 6240.
(83) Because of the overlap of bends and stretch in the powder spectra, assignment in this case is one that remains ambiguous even after the use of isotopic labeling.
(84) Hori, H.; Kitagawa, T. *J. Am. Chem. Soc.* **1980**, *102*, 3608.
(85) Teraoka, J.; Kitagawa, T. *J. Biol. Chem.* **1981**, *256*, 3969.
(86) Salmeen, I.; Rimai, L.; Babcock, G. T. *Biochemistry* **1978**, *17*, 800.
(87) Kitagawa, T.; Nagai, K.; Tsubaki, M. *FEBS Lett.* **1979**, *104*, 376.
(88) Argade, P. V.; Sassaroli, M.; Rousseau, D. L.; Inubushi, T.; Ikeda-Saito, M.; Lapidot, A. *J. Am. Chem. Soc.* **1984**, *106*, 6593.
(89) Matsukawa, S.; Kawatari, K.; Yoneyama, Y.; Kitagawa, T. *J. Am. Chem. Soc.* **1985**, *107*, 1108.
(90) Hashimoto, S.; Teraoka, J.; Inubushi, T.; Yonetani, T.; Kitagawa, T. *J. Biol. Chem.* **1986**, *261*, 11110.
(91) Babcock, G. T.; Ingle, R. T.; Oertling, W. A.; Davis, J. C.; Averill, B. A.; Hulse, C. L.; Stufkens, D. J.; Bolscher, B. G. J. M.; Wever, R. *Biochim. Biophys. Acta* **1985**, *828*, 58.
(92) Manthey, J.; Boldt, N. J.; Bocian, D. F.; Chan, S. I. *J. Biol. Chem.* **1986**, *261*, 6734.
(93) Deinum, G.; Stone, J. R.; Babcock, G. T.; Marletta, M. A. *Biochemistry* **1996**, *35*, 1540.
(94) Kitagawa, T. In *Biological Applications of Raman Spectroscopy*; Spiro, T. G., Ed.; John Wiley and Sons, Inc.: New York, 1988; pp 97−132.
(95) Hu, C.; Peng, Q.; Silvernail, N. J.; Barabanschikov, A.; Zhao, J.; Alp, E. E.; Sturhahn, W. J.; Sage, J. T.; Scheidt, W. R. *Inorg. Chem.* **2013**, *52*, 3170.
(96) Lauraeus, M.; Wikstrom, M.; Varotsis, C.; Tecklenburg, M. M.; Babcock, G. T. *Biochemistry* **1992**, *31*, 10054.
(97) (a) Einarsdóttir, O.; Dyer, R. B.; Killough, P. M.; Fee, J. A.; Woodruff, W. H. *Proc. SPIE* **1989**, *1055*, 254. (b) Einarsdóttir, O.; McDonald, W.; Funatogawa, C.; Szundi, I.; Woodruff, W. H.; Dyer, R. B. *Biochim. Biophys. Acta* **2015**, *1847*, 109.
(98) Wyllie, G. R. A.; Schulz, C. E.; Scheidt, W. R. *Inorg. Chem.* **2003**, *42*, 5722.
(99) Lehnert, N.; Sage, J. T.; Silvernail, N.; Scheidt, W. R.; Alp, E. E.; Sturhahn, W.; Zhao, J. *Inorg. Chem.* **2010**, *49*, 7197.
(100) Li, J.; Peng, Q.; Barabanchikov, A.; Pavlik, J. W.; Alp, E. E.; Sturhahn, W.; Zhao, J.; Schulz, C. E.; Sage, J. T.; Scheidt, W. R. *Chem.—Eur. J.* **2011**, *17*, 11178.

(101) Li, J.; Noll, B. C.; Oliver, A. G.; Schulz, C. E.; Scheidt, W. R. *J. Am. Chem. Soc.* **2013**, *135*, 15627.
(102) Linder, D. P.; Rodgers, K. R. *Inorg. Chem.* **2005**, *44*, 1367.
(103) Serres, R. G.; Grapperhaus, C. A.; Bothe, E.; Bill, E.; WeyhermŸller, T.; Neese, F.; Wieghardt, K. *J. Am. Chem. Soc.* **2004**, *126*, 5138.
(104) Bade, D.; Parak, F. *Z. Naturforsch.* **1978**, *33c*, 488.
(105) Lanucara, F.; Chiavarino, B.; Crestoni, M. E.; Scuderi, D.; Sinha, R. K.; Matre, P.; Fornarini, S. *Inorg. Chem.* **2011**, *50*, 4445.